Water Oxidation

DOI: 10.1002/anie.201408854

Copper as a Robust and Transparent Electrocatalyst for Water Oxidation**

Jialei Du, Zuofeng Chen, Shengrong Ye, Benjamin J. Wiley, and Thomas J. Meyer*

Abstract: *Copper metal is in theory a viable oxidative electrocatalyst based on surface oxidation to Cu^{III} and/or Cu^{IV}, but its use in water oxidation has been impeded by anodic corrosion. The in situ formation of an efficient interfacial oxygen-evolving Cu catalyst from Cu^{II} in concentrated carbonate solutions is presented. The catalyst necessitates use of dissolved Cu^{II} and accesses the higher oxidation states prior to decompostion to form an active surface film, which is limited by solution conditions. This observation and restriction led to the exploration of ways to use surface-protected Cu metal as a robust electrocatalyst for water oxidation. Formation of a compact film of CuO on Cu surface prevents anodic corrosion and results in sustained catalytic water oxidation. The Cu/CuO surface stabilization was also applied to Cu nanowire films, which are transparent and flexible electrocatalysts for water oxidation and are an attractive alternative to ITO-supported catalysts for photoelectrochemical applications.*

A central thrust in energy research at present focuses on bioinspired artificial photosynthesis and the development of solar-driven chemical reactors that are capable of using sunlight to synthesize molecular fuels.[1–4] In these schemes, water oxidation ($2H_2O \rightarrow O_2 + 4e^- + 4H^+$, $E^{o\prime} = 1.23\,V - 0.059\,(pH)\,V$ vs. NHE) is the essential other half-reaction. It provides reductive equivalents for conversion of CO_2 into CO or other reduced forms of carbon, or H_2O/H^+ to hydrogen.[1–4] Research on water oxidation catalysis has focused on lowering overpotentials, reducing cost with earth abundant elements, and critically, improving long-term oxidative stability by circumventing thermodynamically unstable organic ligands. In nature, the fine-tuned molecular machinery of the oxygen-evolving complex (OEC) in green leaves oxidizes water using a Mn_4O_4Ca cluster.[5,6] Related artificial examples include pre-prepared Mn oxide clusters,[7] Co and Ni clusters that form spontaneously in solution,[8,9] Co_3O_4 (spinel) particles,[10] colloidal $IrO_2 \cdot n\,H_2O$,[11] and amorphous iridium oxide deposited from organometallic precursors.[12] Pt electrodes and some precious metal oxides have also been reported to function as electrocatalyts,[13,14] but they are neither abundant nor inexpensive.

In solar fuel production, copper metal has been the focus of most CO_2 reduction studies,[15,16] but its direct use as an electrocatalyst for water oxidation has been largely impeded by severe anodic corrosion. The anodic reactions of copper metal are surprisingly complex, involving both soluble and insoluble products and multiple oxidation states with Cu^{I}, Cu^{II}, Cu^{III}, and/or Cu^{IV}, which are all invoked depending on the applied potential. For the $Cu^{I/0}$ and $Cu^{II/I}$ couples, $E(Cu^{+/0}) = 0.159$ V and $E(Cu^{2+/0}) = 0.34$ V. In general, the deterioration of copper is pronounced in solutions of low pH but becomes relatively sluggish at increasing pH owing to the formation of protective films on the metallic surface.[17,18]

Recently, we reported efficient and sustained electrocatalytic water oxidation based on simple Cu^{II} salts in concentrated carbonate (1M, pH 10.8) aqueous solutions.[19] High concentrations of carbonate anions are essential in providing proton acceptor bases and complex ion formation (for example, $[Cu^{II}(\eta^2\text{-}O_2OC)_2(OH_2)_2]^{2-}$) to avoid precipitation of $Cu(OH)_2$ ($K_{sp} = 2.2 \times 10^{-20}$) or $CuCO_3$ (1.4×10^{-10}).[20] Electron-donating carbonate ligands also lower potentials for accessing higher-oxidation-state Cu^{III} and/or Cu^{IV} oxo-ligand oxidized intermediates. Although water oxidation catlaysis under these conditions is dominated by homogeneous complexes, preliminary results were obtained for interfacial catalysis of water oxidation by an electroactive surface precipitate.[19] Formation of the active layer and interfacial water oxidation catalysis are dependent on the concentration of Cu^{II} and carbonate. For example, during electrolysis in 1M Na_2CO_3, the surface precipitate appeared only at high Cu^{II} concentrations (≥ 0.8 mM), pointing to surface equilibrium formation between solution precursors and precipitated film. Decreasing the carbonate concentration to about 0.1M resulted in decreased Cu^{II} solubility. Increasing the concentration to about 2M resulted in termination of water oxidation owing to complete coordination by carbonate, which removes the co-ordination of aqua ligand(s) on Cu^{II}.[19]

Herein, we report the in situ formation of a robust, efficient interfacial oxygen-evolving Cu catalyst from Cu^{II} in solution, leading to surface-modified Cu metal electrodes for sustained water oxidation. Formation of a compact film of CuO with incorporated $Cu(OH)_2$ on the underlying copper is found to prevent electro-corrosion, allowing for sustained catalytic water oxidation without surface degradation. In

[*] J.-L. Du, Prof. Z.-F. Chen
Department of Chemistry, Tongji University
Shanghai 200092 (China)
E-mail: zfchen@tongji.edu.cn
Dr. S.-R. Ye, Prof. B. J. Wiley
Department of Chemistry, Duke University
Durham, NC 27708 (USA)
Prof. T. J. Meyer
Department of Chemistry
University of North Carolina at Chapel Hill
Chapel Hill, NC 27599 (USA)

[**] Z.F.C. thanks the support of the National Natural Science Foundation of China (21405114) and The Recruitment Program of Global Youth Experts by China.

Supporting information for this article is available on the WWW under http://dx.doi.org/10.1002/anie.201408854.

contrast to Cu^{II}/precipitate catalysis reported in the earlier study, Cu/CuO catalysis is no longer limited by the solubility and diffusion of Cu^{II} in solution, or by the coordination environment needed for higher-oxidation-state film formation. The robust Cu/CuO surfaces for water oxidation have been extended to copper nanowire networks providing transparent, flexible electrocatalysts for possible applications in photoelectrochemical cells (PECs).

In a typical experiment with 3 mM Cu^{II} in 1 M Na_2CO_3 (pH 10.8), constant potential electrolysis at 1.30 V vs. NHE resulted in a visible surface precipitate on ITO electrodes. As noted above, at these carbonate and Cu^{II} concentrations, an interfacial oxygen-evolving Cu catalyst is deposited. The film thickness gradually increased over the course of the electrodeposition. A maximum activity under these conditions was achieved after 4–6 h of electrolysis.

Figure 1 A,B shows that the surface-bound solid is active toward water oxidation in 1 M Na_2CO_3 (pH 10.8). In cyclic voltammograms (CVs), scanning the electrode beyond about 0.98 V results in a dramatic current enhancement with an

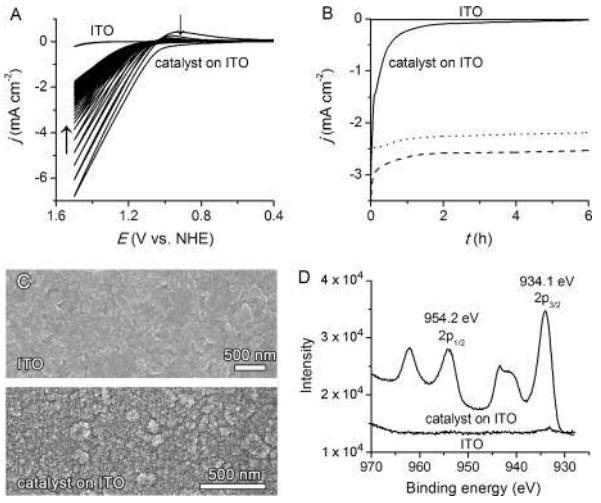

Figure 1. A) CVs (25 scan cycles) of the precipitated film and bare ITO electrode in 1 M Na_2CO_3 (pH ≈ 10.8). The arrows indicate a current decrease during successive CV scans. B) As in (A), controlled potential electrolysis of the precipitated film and bare ITO at 1.20 V vs. NHE. Sustained electrolysis with 0.8 mM added Cu^{2+} (•••••) or by increasing the pH from 10.8 to 11.7 (-----) are also shown. C) SEM images and D) XPS spectra of Cu species on ITO electrode before and after electrolysis to form the precipitated film. The formation of a precipitated film on ITO electrode was achieved by constant potential electrolysis in 1 M Na_2CO_3 (pH 10.8) containing 3 mM Cu^{2+} at 1.30 V vs. NHE for 6 h.

overpotential of about 0.39 V at the current onset ($E_{p,o}$) for water oxidation. In the reverse scan, a current cross-over appears along with small re-reduction waves at $E_{p,c} \approx 1.0$–0.70 V. These observations indicate that oxygen evolution is activated following catalyst oxidation to a higher oxidation state, which undergoes a structural change with re-reduction occurring at a more negative potential. The decrease in catalytic current during successive CV scans and constant potential electrolysis (Figure 1 B, solid curve) is attributable to re-dissolution of film into the 1 M Na_2CO_3 (pH 10.8) solutions. Sustained catalysis can be achieved by adding small amounts of Cu^{2+} (e.g. 0.8 mM) in solution to compensate for the dissolution of the surface-bound solid (dotted line). In earlier reports, a self-repair mechanism was proposed for sustained electrocatalytic water oxidation by CoO_xH_y or NiO_xH_y clusters and/or films formed in situ from added Co^{II} or Ni^{II}.[8,9] Sustained catalysis can also be achieved by increasing the pH from 10.8 to 11.7 with NaOH (dashed line). The higher stability of the cluster film at higher pH is generally consistent with the pH-dependent performance of Co-based catalysts. Studies on cobalt-based water oxidation revealed heterogeneous catalysis at pH > 3.5, but the precipitated film does not form or is prone to dissove at lower pH.[21]

Scanning electron microscopy (SEM) shows that the electrodeposited material consists of particles with diameters in the tens to hundreds of nanometers range that have coalesced into a thin film (Figure 1 C). The X-ray powder diffraction pattern (XRD) of an electrodeposited catalyst shows broad amorphous features and no peaks indicative of crystalline phases other than the peaks associated with the ITO underlayer (Supporting Information, Figure S1).

In the absence of detectable crystallites, the composition of the surface precipitate at ITO electrodes was analyzed by X-ray photoelectron spectroscopy (XPS) combined with Raman spectroscopy. The disappearance of In $3d_{3/2}$ and $3d_{5/2}$ signals for ITO after electrolysis (Supporting Information, Figure S2) is consistent with the fact that the ITO substrate is completely covered with the precipitated film. In Figure 1 D, XPS of the Cu-based precipitate after electrolysis includes a set of peaks consisting of $2p_{3/2}$ and $2p_{1/2}$ peaks at 934.1 eV and 954.2 eV with additional intense satellite peaks characteristic of Cu^{II}.[22] There is a clear similarity to CuO but with the energies shifted toward higher binding energies by 0.5–0.6 eV, which is most likely due to the presence of some $Cu(OH)_2$ in the film.[22] $Cu(OH)_2$ has a 2p binding energy that is circa 0.8 eV higher than that of CuO.[22] Consistent with XPS results, a broad Raman band is observed at about 561 nm (Supporting Information, Figure S3), which is located between the dominant Raman peaks of CuO (640 nm) and $Cu(OH)_2$ (480 nm).[23] Further characterization of the solid is underway, but the film that forms during water oxidation electrolysis in 1 M $NaCO_3$ appears to be a surface-accumulated copper(II) deposit dominated by amorphous CuO incorporating a substantial amount of $Cu(OH)_2$.

The observation of the in situ formed, interfacial oxygen-evolving, precipitated Cu^{II} water oxidation catalyst led us to explore ways to use surface-protected copper metal as a direct water oxidation electrocatalyst. Figure 2 A (see also the Supporting Information, Figure S4) show successive CVs of a clean copper foil (0.6 cm^2) in 1 M Na_2CO_3 solution (pH ≈ 10.8). During the first scan cycle, an anodic wave appears which extends from about 0.2 to about 0.95 V. Surface processes at the copper electrode in this potential region are due to surface oxidation.[17,18] During the second oxidative cycle, the oxidative wave disappeared with stable and reproducible CV scans obtained thereafter. This observation is consistent with oxidation during the first scan cycle forming

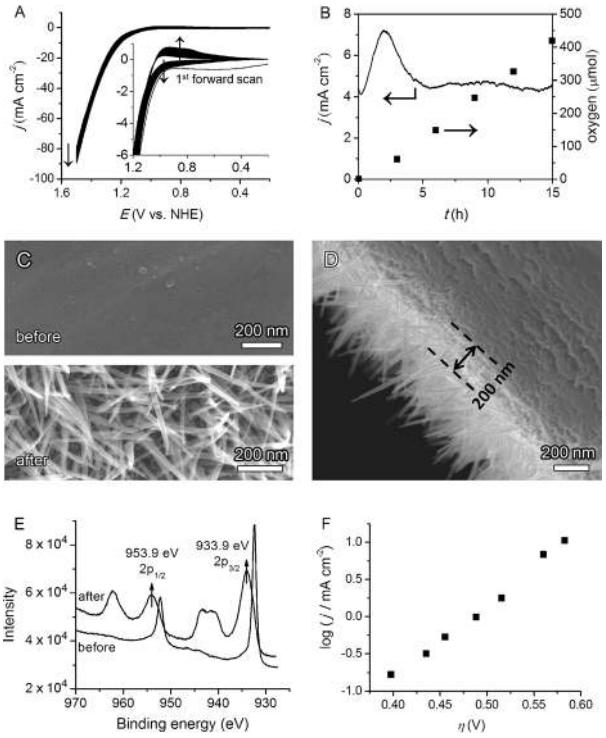

Figure 2. A) CVs (25 scan cycles) of a Cu foil electrode in 1 M Na_2CO_3 (pH ≈ 10.8). Scan rate 100 mV s^{-1}. The arrows indicate a slight current enhancement during successive CV scans. Inset: a magnified view of the CVs. B) Constant potential electrolysis and oxygen production with a Cu foil in 1 M Na_2CO_3 (pH ≈ 10.8) at 1.20 V vs. NHE. C) Top-down and D) cross-sectional SEM images of a Cu foil before and after sustained water oxidation. E) XPS spectra of a Cu foil before and after sustained water oxidation. F) Tafel plot, $\eta = (V_{appl} - iR) - E(\text{pH } 10.8)$ (where V_{appl} is the applied potential), of a Cu foil electrode in 1 M Na_2CO_3 (pH ≈ 10.8), corrected for the *iR* drop in the solution.

a protective, passivating layer.[18] The results cited below were obtained following the first scan cycle.

Further scanning the electrode results in a dramatic current enhancement with $E_{p,o} \approx 0.96$ V, an overpotential of about 0.37 V for water oxidation. In the reverse scan, a current cross-over appears along with small re-reduction waves at $E_{p,c} \approx 1.0$–0.70 V. The overall behavior is similar to that for the in situ catalyst film shown in Figure 1 A, but catalytic currents and peak currents for re-reduction are increased slightly duing successive scans and the catalytic current density for water oxidation is 5–10 times higher. Additional CV data at different scan rates, in D_2O/H_2O water, and in a CH_3CN/H_2O mixture are shown in the Supporting Information, Figures S5–S7.

Figure 2 B shows the results of a controlled potential electrolysis conducted at 1.20 V. The electrolysis current dropped slightly in magnitude initially. As the surface was being activated, the catalytic current increased gradually, reaching a maximum value of 7 mA cm^{-2} after 2 h. Further extension of the electrolysis period resulted in a decrease in catalytic current until it stabilized at a level of about 4.3 mA cm^{-2} after about 5 h. During the electrolysis, a dark coating developed on the copper foil surface. Although the active film is necessary for catalytic water oxidation, a gradually increasing film thickness may block rapid electron transfer to the underlying Cu substrate resulting in the decrease in catalytic current during the film development. The appearance of sustained catalytic currents after about 5 h provides evidence for stable catalytic films. Vigorous effervescence was observed at the electrode surface during the electrolysis. Product analysis by an oxygen probe (YSI ProODO) gave 420 μmol of O_2 over an electrolysis period of 15 hours with a Faradaic efficiency of 98% for O_2 production. The amount of charge passed (166 C, 1.72 mmol) during 15 h electrolysis period far exceeds what could be accounted for by the total loss of copper into solution and the formation of surface-bound copper layer (1.9 μmol copper in total).

The SEM images of the Cu foil electrode in Figure 2 C,D (see also the Supporting Information, Figure S8) show that the Cu foil greatly increased in roughness after water oxidation. The surface was covered by a compact layer that prevents the anodic corrosion of the underlying copper during water oxidation. The compact layer consists of a nanoparticle/nanocluster film with particles having diameters in the tens of nanometers (top-down) and a thickness of about 200 nm (cross-sectional). There is evidence in the SEM images for grass-like structures with a diameter of about 30 nm and a length of about 300 nm growing from the nanoparticle layer. This morphology could contribute to a significantly enhanced effective surface area and the increases in catalytic current observed relative to the precipitated films on ITO.

XRD measurement on the developed dark film failed to detect any new peaks indicative of crystalline phases other than those for underlying bulk Cu (Supporting Information, Figure S9). XPS of an untreated Cu foil (Figure 2 E) exhibits two peaks at 932.0 and 951.8 eV, characteristic of the $2p_{3/2}$ and $2p_{1/2}$ binding energies of Cu^0 metal.[22] After water oxidation, the 2p peaks shift to 933.9 eV and 953.9 eV with additional rounded features appearing in the spectra. As for the precipitated film in Figure 1 D, the profile of the XPS spectrum is generally similar to that for CuO[22] but with the 2p binding energies higher in energy by 0.3 eV, which is most likely due to the presence of some $Cu(OH)_2$ in the film.

Figure 2 F shows current density (j) for water oxidation at a Cu foil as a function of overpotential (η) in 1 M Na_2CO_3 solution (pH ≈ 10.8). The measurements were conducted on a copper foil that had been activated by pre-electrolysis in 1 M Na_2CO_3 (pH ≈ 10.8) at 1.20 V for 2 h. The surface treatment resulted in maximum catalytic currents as shown in Figure 2 B. The slope of a plot of log(j) vs. η was about 90 mV/decade for current densities ranging from 0.1 mA cm^{-2} to 10 mA cm^{-2}. An appreciable catalytic current (≥ 0.1 mA cm^{-2}) is observed beginning at $\eta = 380$ mV. Current densities of 1 and 10 mA cm^{-2} were obtained at $\eta = 485$ mV and 580 mV, respectively, with a target of 10 mA cm^{-2} for ambient solar applications. This activity is superior to other copper-based electrocatalysts attributable to a nanostructural morphology.[24–27]

Relatively concentrated solutions of CO_3^{2-} play a key role in preventing electro-corrosion of the copper foil during water oxidation. Adding 0.5 M Na_2SO_4 to 1 M Na_2CO_3 (pH 10.8) results in no observable changes in the CV.

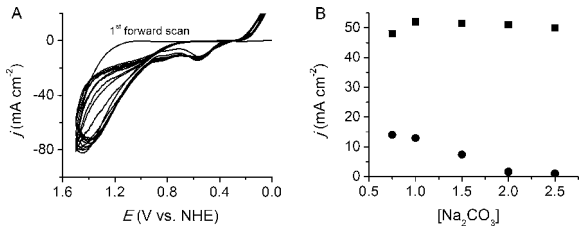

Figure 3. A) CVs (10 successive scan cycles) of a Cu foil electrode in 0.5 M Na_2CO_3 (pH 10.8) with 0.5 M Na_2SO_4. B) Plot of catalytic current density from CVs of 100 $mV s^{-1}$ at 1.40 V versus the concentration of Na_2CO_3. ● 3 mM $CuSO_4$ at a boron-doped diamond electrode, ■ at a Cu foil electrode without $CuSO_4$.

However, in 0.5 M Na_2CO_3 with 0.5 M added Na_2SO_4, severe electro-corrosion occurs. As shown in Figure 3 A, successive CVs in this solution feature a roughened surface with the appearance of surface oxidative waves. During these scans, the rapid dissolution of the copper foil resulted in a blue flocculate around the electrode. Figure S10 shows that the copper foil is severely etched after only 50 successive CV scans in the solution mixture of 0.5 M Na_2CO_3 and 0.5 M Na_2SO_4. Similar phenomena were also observed with other added inorganic salts, namely NaCl, $NaNO_3$, and $NaClO_4$. In contrast, the copper foil remained intact in 1 M Na_2CO_3 after 500 successive CV scans with the surface covered with a compact dark layer, which was the basis for sustained catalytic water oxidation. The effect of added inorganic salts in accelerating electro-corrosion of copper is complex and may be related to initial anion adsorption or coordination to the copper surface, which inhibits the formation of and/or destroys the passivated compact layer of CuO intermediate during water oxidation.

In Cu^{II} catalysis, the catalytic current density decreases with increasing carbonate concentration owing to complete coordination by carbonate.[19] In this case, as found for single site polypyridyl Ru[28,29] and Ir[30,31] complexes [Eq. (1)], the presence of aqua or hydroxo ligands is an important feature for water oxidation catalysis, probably by providing access to high oxidation state Cu-oxo intermediates by proton-coupled electron transfer (PCET) prior to its decomposition to form the surface precipitate [Eq. (2)]. Therefore, a balance between enhanced solubility of added Cu^{II} salts and impact on reactivity must be considered and balanced. By comparison, the catalytic film developed from the underlying copper metal and the catalysis are not limited by carbonate concentration. As shown in Figure 3 B, the catalytic current is nearly unchanged over a carbonate concentration range of 0.5 M to 2.5 M.

$$[Ru^{II}-OH_2]^{2+} \xrightarrow{-e^-,\,-H^+} [Ru^{III}-OH]^{2+} \xrightarrow{-e^-,\,-H^+} [Ru^{IV}=O]^{2+} \xrightarrow{-e^-} [Ru^{V}=O]^{3+} \quad (1)$$

$$[Cu^{II}-OH_2]^{2+} \xrightarrow{-e^-,\,-H^+} [Cu^{III}\text{-}OH]^{2+} \xrightarrow{-e^-,\,-H^+} [Cu^{IV}=O]^{2+} ([Cu^{III}-O^{\bullet}]^{2+}) \quad (2)$$

An important consideration in the design of PECs is that the water-splitting catalysts do not obstruct the transmission of light to the dye or photovoltaic elements of the device.[2,32,33] Currently, most designs of PECs rely on ITO as the transparent conductor coated by an active layer of catalyst: CoO_x or NiO_x for water oxidation. However, indium is not abundant, and ITO film is brittle and expensive.[34,35] Copper nanowires (Cu NWs) are an attractive alternative to ITO because they can be deposited from solution at rates several orders of magnitude faster than gas-phase ITO sputtering, offer nearly the same level of optoelectric performance, and copper is 100 times cheaper than indium.[36–38] As shown here, Cu can be robust toward water oxidation in concentrated carbonate solutions, and we explored an additional application with the direct use of a Cu nanowire film, involving no pre-coated catalytic layer such as Ni or Co,[33] as a transparent electrocatalyst for water oxidation, potentially as a replacement for ITO in PECs.

Cu NWs (> 20 μm in length and about 70 ± 25 nm in diameter) were synthesized and coated onto glass by Meyer rod (see the Supporting Information).[39] Figure 4 A,C,E shows dark-field optical microscopy (DFOM), SEM, and transmission electron microscopy (TEM) images of Cu NW networks, respectively. They show that the Cu NWs are evenly dispersed across the glass substrate and interconnected. The Cu NW film (65 $mg m^{-2}$) exhibited a sheet resistance of 30 Ωsq^{-1} with a specular transmittance of 85% (λ = 550 nm). The transmittance and sheet resistance of a NW film can be varied by simply changing the areal density of the NWs.[39]

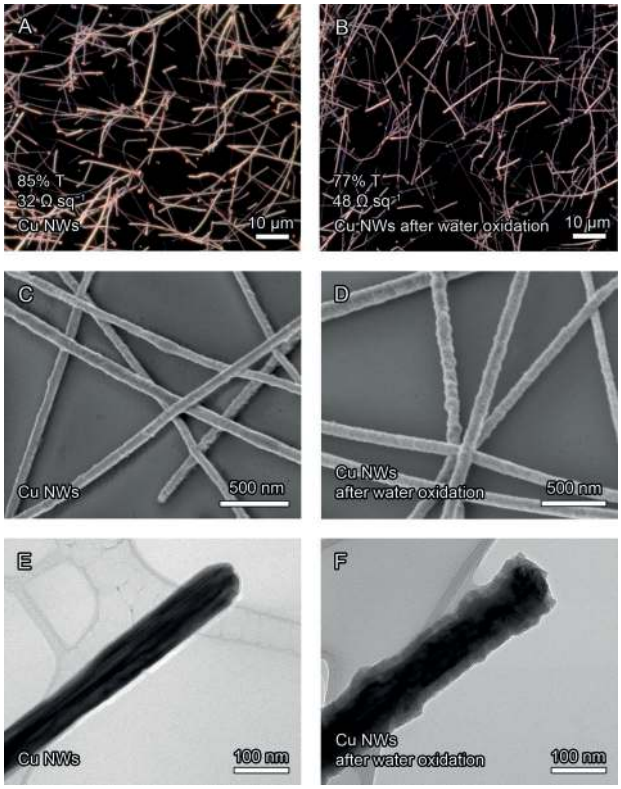

Figure 4. Dark-field optical microscopy (A,B), SEM (C,D), and TEM (E,F) images of Cu NWs (A,C,E) and Cu NWs after sustained water oxidation (B,D,F) in Figure 5 B.

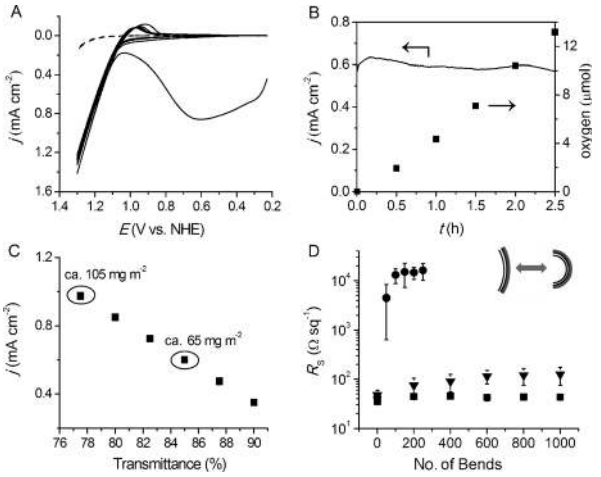

Figure 5. A) CVs (10 scan cycles) of a Cu NW network on glass (1.0 cm^2) in 1 M Na_2CO_3 (pH ≈ 10.8). Scan rate 100 $mV s^{-1}$. For comparison, a CV of an ITO electrode is shown as a dashed line. B) Constant potential electrolysis with a Cu NW network at 1.20 V vs. NHE with 0.8 mM $CuSO_4$ added to the solution. C) A plot of the transmittance of Cu NW networks vs. catalytic current density of water oxidation. D) Plots of sheet resistance (R_S) versus number of bends for ● ITO film, ■ Cu NW film, and ▼ Cu NW film after water oxidation on PET.

Figure 5A shows CVs of a Cu NW film in 1 M Na_2CO_3 (pH ≈ 10.8). As for the Cu foil in Figure 2A, an anodic peak(s) appears on oxidative scanning that extends from about 0.2 to about 1.0 V during the first scan cycle but disappears in the second cycle. Repeated catalytic waves for water oxidation were observed with $E_{p,o} = 1.02$ V vs. NHE. For comparison, only a small oxygen evolution wave was observed at ITO electrodes under identical condtions. The low activity of ITO necessitates the coating of an active layer of catalyst such as CoO_x or NiO_x, which imposes a trade-off between catalytic activity and light transmission.[2,32]

Figure 5B shows that electrolysis proceeds with a stable current density level of about 0.6 $mA cm^{-2}$ at 1.20 V. Over the 2.5 h electrolysis period, about 13.2 μmol of O_2 was generated with a columbic efficiency of about 94%. The Cu NW networks were intact with a slight increase in surface roughness after sustained water oxidation (Figure 4B,D,F), and a distinct core–shell structure of the NW was observed owing to formation of an active catalytic layer of thickness 18 ± 5 nm. The film maintained excellent optical (77%) and electrical (48 Ω sq^{-1}) properties. Addition of a dilute solution of Cu^{II} is essential for sustained, long-term electrolysis at the Cu NW networks, consistent with a self-repair mechanism.[8,9] With no added Cu^{II} ions in the solution, the Cu NWs gradually dissolved by oxidation after prolonged electrolysis, resulting in decreasing catalytic current densities and decomposition of the networks.

The catalytic current density of the Cu NW network could be further enhanced by increasing the density of nanowires on the substrate. As shown in Figure 5C, the current density increases linearly with the NW loading. A current density of about 1 $mA cm^{-2}$ was achieved by increasing the areal density of Cu NWs to about 105 $mg m^{-2}$ (< 15 Ω sq^{-1}, 77.5% at 550 nm). The trend in Figure 5C suggests an even higher catalytic current density can be attained at the expense of film transmittance.

Films made from metal nanowires are generally much more flexible that films of ITO. To demonstrate this fact in this case, we prepared Cu NW networks on polyethylene terephthalate (PET), a plastic substrate widely used for flexible, transparent conductive films. As shown in the Supporting Information, Figure S11, the catalytic activity of Cu NW film toward water oxidation is virtually the same on PET as it is on glass. Cu NW films on PET were previously bent 1000 times, with little degradation in sheet resistance (30 to 40 Ω sq^{-1}).[39] To confirm that the flexibility is retained after water oxidation, a Cu NW film after water oxidation was repeatedly bent from a 10 mm to a 2.5 mm radius of curvature. Figure 5D shows that the sheet resistance of the film increased slightly from 30 to 125 Ω sq^{-1} after 1000 bends. This is in contrast to the ITO film on PET, for which the sheet resistance increased 400 times after just 250 bends. Considering the low cost and design flexibility of transparent plastics compared to glass, the extension to plastic substrates could enable new, versatile, and lower cost design architectures for solar fuel devices.

In conclusions, harnessing the potenital of artificial photosynthesis at the required scale will require inexpensive, easily fabricated devices that are robust and inexpensive to manufacture and operate under ambient conditions. The results reported here highlight the use of earth-abundant, surface-protected copper as a robust water oxidation electrocatalyst in concentrated carbonate solution. Current densities of 1 and 10 $mA cm^{-2}$ were obtained at overpotentials of 485 mV and 580 mV, respectively. Becasue of the robustness of Cu in these solutions, Cu nanowire films were prepared and demonstrated to act as transparent electrocatalysts for water oxidation, making them an attractive alternative to ITO-supported catalysts for photoelectrochemical cells. Moreover, the relatively greater flexibility of nanowire films may expand the design space for the devices.

Considering that copper metal is also unique among solid electrode materials in its ability to reduce CO_2,[15,16] there may be additional implications of these results for alternate solar-fuel strategies, for example, with Cu metal electrodes or Cu nanowire networks in a two-compartment cell used for catalytic CO_2 splitting, $CO_2 \rightarrow CO + {}^1/_2 O_2$, with the half-reactions $H_2O - 2e^- \rightarrow {}^1/_2 O_2 + 2H^+$ at the anode and $3CO_2 + H_2O + 2e^- \rightarrow CO + 2HCO_3^-$ at the cathode and an ion-exchange membrane to maintain the charge and mass balance and separate the produced gases. The simplicity of the catalytic system described herein meets the requirements for deploying a solar fuels strategy on a large scale.

Received: September 5, 2014
Revised: November 4, 2014
Published online: January 7, 2015

Keywords: copper · electrocatalysis · heterogeneous catalysis · transparent electrodes · water oxidation

[1] T. R. Cook, D. K. Dogutan, S. Y. Reece, Y. Surendranath, T. S. Teets, D. G. Nocera, *Chem. Rev.* **2010**, *110*, 6474 – 6502.
[2] M. G. Walter, E. L. Warren, J. R. McKone, S. W. Boettcher, Q. Mi, E. A. Santori, N. S. Lewis, *Chem. Rev.* **2010**, *110*, 6446 – 6473.
[3] D. Gust, T. A. Moore, A. L. Moore, *Acc. Chem. Res.* **2009**, *42*, 1890 – 1898.
[4] J. H. Alstrum-Acevedo, M. K. Brennaman, T. J. Meyer, *Inorg. Chem.* **2005**, *44*, 6802 – 6827.
[5] K. N. Ferreira, T. M. Iverson, K. Maghlaoui, J. Barber, S. Iwata, *Science* **2004**, *303*, 1831 – 1838.
[6] J. Yano, J. Kern, K. Sauer, M. J. Latimer, Y. Pushkar, J. Biesiadka, B. Loll, W. Saenger, J. Messinger, A. Zouni, V. K. Yachandra, *Science* **2006**, *314*, 821 – 825.
[7] I. Zaharieva, P. Chernev, M. Risch, K. Klingan, M. Kohlhoff, A. Fischer, H. Dau, *Energy Environ. Sci.* **2012**, *5*, 7081 – 7089.
[8] M. W. Kanan, D. G. Nocera, *Science* **2008**, *321*, 1072 – 1075.
[9] M. Dinca, Y. Surendranath, D. G. Nocera, *Proc. Natl. Acad. Sci. USA* **2010**, *107*, 10337 – 10341.
[10] F. Jiao, H. Frei, *Angew. Chem. Int. Ed.* **2009**, *48*, 1841 – 1844; *Angew. Chem.* **2009**, *121*, 1873 – 1876.
[11] W. J. Youngblood, S. H. A. Lee, Y. Kobayashi, E. A. Hernandez-Pagan, P. G. Hoertz, T. A. Moore, A. L. Moore, D. Gust, T. E. Mallouk, *J. Am. Chem. Soc.* **2009**, *131*, 926 – 927.
[12] J. D. Blakemore, N. D. Schley, G. W. Olack, C. D. Incarvito, G. W. Brudvig, R. H. Crabtree, *Chem. Sci.* **2011**, *2*, 94 – 98.
[13] S. Trassati in *Electrochemistry of Novel Materials* (Eds.: J. Lipkowski, P. N. Ross), VCH, New York, **1994**, chap. 5.
[14] M. R. Tarasevich, B. N. Efremov in *Electrodes of Conductive Metal Oxides* (Ed.: S. Trasatti), Elsevier, Amsterdam, **1980**, chap. 5.
[15] Y. Hori, A. Murata, R. Takahashi, *J. Chem. Soc. Faraday Trans. 1* **1989**, *85*, 2309 – 2326.
[16] C. W. Li, M. W. Kanan, *J. Am. Chem. Soc.* **2012**, *134*, 7231 – 7234.
[17] G. Kear, B. D. Barker, F. C. Walsh, *Corros. Sci.* **2004**, *46*, 109 – 135.
[18] L. D. Burke, M. J. G. Ahern, T. G. Ryan, *J. Electrochem. Soc.* **1990**, *137*, 553 – 561.
[19] Z. F. Chen, T. J. Meyer, *Angew. Chem. Int. Ed.* **2013**, *52*, 700 – 703; *Angew. Chem.* **2013**, *125*, 728 – 731.
[20] P. Patnaik, *Handbook of Inorganic Chemicals*, McGraw-Hill, New York, **2002**.
[21] J. B. Gerken, J. G. McAlpin, J. Y. C. Chen, M. L. Rigsby, W. H. Casey, R. D. Britt, S. S. Stahl, *J. Am. Chem. Soc.* **2011**, *133*, 14431 – 14442.
[22] C. D. Wanger, W. M. Riggs, L. E. Davis, J. F. Moulder, G. E. Muilenberg in *Handbook of x-ray photoelectron spectroscopy: a reference book of standard data for use in x-ray photoelectron spectroscopy*, PerkinElmer Corp., Physical Electronics Division, Eden Prairie, Minnesota, USA, **1979**, p. 82.
[23] S. T. Mayer, R. H. Muller, *J. Electrochem. Soc.* **1992**, *139*, 426 – 434.
[24] X. Liu, H. Jia, Z. Sun, H. Chen, P. Xu, P. Du, *Electrochem. Commun.* **2014**, *46*, 1 – 4.
[25] S. M. Barnett, K. I. Goldberg, J. M. Mayer, *Nat. Chem.* **2012**, *4*, 498 – 502.
[26] T. Zhang, C. Wang, S. B. Liu, J. L. Wang, W. B. Lin, *J. Am. Chem. Soc.* **2014**, *136*, 273 – 281.
[27] M.-T. Zhang, Z. Chen, P. Kang, T. J. Meyer, *J. Am. Chem. Soc.* **2013**, *135*, 2048 – 2051.
[28] Z. F. Chen, J. J. Concepcion, X. Q. Hu, W. T. Yang, P. G. Hoertz, T. J. Meyer, *Proc. Natl. Acad. Sci. USA* **2010**, *107*, 7225 – 7229.
[29] J. J. Concepcion, J. W. Jurss, M. K. Brennaman, P. G. Hoertz, A. O. T. Patrocinio, N. Y. M. Iha, J. L. Templeton, T. J. Meyer, *Acc. Chem. Res.* **2009**, *42*, 1954 – 1965.
[30] N. D. McDaniel, F. J. Coughlin, L. L. Tinker, S. Bernhard, *J. Am. Chem. Soc.* **2008**, *130*, 210 – 217.
[31] J. F. Hull, D. Balcells, J. D. Blakemore, C. D. Incarvito, O. Eisenstein, G. W. Brudvig, R. H. Crabtree, *J. Am. Chem. Soc.* **2009**, *131*, 8730 – 8731.
[32] S. Y. Reece, J. A. Hamel, K. Sung, T. D. Jarvi, A. J. Esswein, J. J. H. Pijpers, D. G. Nocera, *Science* **2011**, *334*, 645 – 648.
[33] Z. Chen, A. R. Rathmell, S. Ye, A. R. Wilson, B. J. Wiley, *Angew. Chem. Int. Ed.* **2013**, *52*, 13708 – 13711; *Angew. Chem.* **2013**, *125*, 13953 – 13956.
[34] U.S. Geological Survey, *Mineral Commodity Summaries. Indium*, **2011**, 74.
[35] M. Aparicio, A. Jitianu, L. C. Klein, *Sol-Gel Processing for Conventional and Alternative Energy*, Springer New York Heidelberg Dordrecht London, **2012**, p. 286.
[36] U. S. Geological Survey, *Mineral Commodity Summaries. Copper*, **2011**, 48.
[37] H. Guo, N. Lin, Y. Chen, Z. Wang, Q. Xie, T. Zheng, N. Gao, S. Li, J. Kang, D. Cai, D.-L. Peng, *Sci. Rep.* **2013**, *3*, 2323.
[38] S. Ye, A. R. Rathmell, I. E. Stewart, Y.-C. Ha, A. R. Wilson, Z. Chen, B. J. Wiley, *Chem. Commun.* **2014**, *50*, 2562 – 2564.
[39] A. R. Rathmell, B. J. Wiley, *Adv. Mater.* **2011**, *23*, 4798 – 4803.

